The Chaotropically Synthesized Dimolybdenum(II,II) Compound*

*Boris Udovic,** Ivan Leban, and Primož Šegedin*

*Faculty of Chemistry and Chemical Technology, University of Ljubljana,
Aškerčeva 5, P. O. Box 537, 1001 Ljubljana, Slovenia*

A non-classic approach in the synthesis and crystal growth within electrostricted water solutions of highly charged ionic species allowed us to obtain bright monocrystals of the zwitterionic tetracarboxylate compound $Mo_2(O_2CC_6H_3(NH_3)_2)_4Cl_8 \cdot 16H_2O$ (**1**). The title compound tetrakis-(μ-3,5-diaminobenzoate)octachlorodimolybdenum(II,II)—aqua(1/16) (**1**) crystallizes in the $P2_1/c$ monoclinic space group with a = 11.0825(13) Å, b = 23.983(3) Å, c = 10.935(6) Å, β = 103.04(3)°, and Z = 2. Proton jumps between aromatic NH_3^+ and the neighbouring contacting groups H_2O or Cl^- of (**1**) increase the extent of donor (p–π) interactions from equatorial oxygen atoms to the central dimolybdenum(II,II) core. Existence of unequivalent carboxylate ligands with different binding affinity around the Mo_2^{4+} dimer is indicated. The structure of the reference compound 3,5-diaminobenzoic acid—bis(hydrogen chloride)—hemihydrate $3,5-(H_2N)_2C_6H_3CO_2H \cdot 2HCl \cdot 1/2H_2O$ (**2**) was solved and compared with the structural data of (**1**). Triclinic needles of (**2**) crystallize in the $P\bar{1}$ space group with a = 8.695(2) Å, b = 9.768(2) Å, c = 13.779(3) Å, α = 67.43(2), β = 68.69(2), γ = 72.66(2)° and Z = 4.

Key words: dimolybdenum tetracarboxylate, tetrakis complex, zwitterionic ligands, chaotropic effects, electrostriction, desymmetrization, quadruply bonded species.

INTRODUCTION

Earlier indications of several important physical-chemical[1] particularities and pharmaceutical[2] activities of dimolybdenum(II,II) coordination compounds stimulate further researches to project water-soluble complexes as zwitterionic forms of aminoacid tetracarboxylates. However, the inherent nucleation and crystal growth of highly soluble and multicharged adducts constitute a continuously open question of how to apply optimal strategies. Although long experienced,[3] the empirically induced salting-in and salting-out effects in protein solutions do not seem to give an efficient approach or a powerful method in crystallization attempts. On the other hand, simple pH adjustments become an unreliable and misleading practice as the »p« functions lose their descriptive property in highly structured matrix-solutions. The dihydrochloric salt of the symmetrical 3,5-diaminobenzoic acid constitutes a useful source of extremely reactive zwitterionic ligands, with high affinity to bind dinuclear dimers as Mo_2^{4+}. The synthesis and the structure of $Mo_2(O_2CC_6H_3(NH_3)_2)_4Cl_8 \cdot 16H_2O$ (**1**) are reported and compared with the reference compound $3,5-(H_2N)_2C_6H_3CO_2H \cdot 2HCl \cdot 1/2H_2O$ (**2**). In several structures of tetracarboxylato-bridged dimetal complexes, some authors[4] assign the idealized point group D_{4h} to the polyhedral oxygen cage O_8 around the Mo_2^4 dimer. In this research, some evidence for the existence of a true dissymmetrical environment around apical Mo atoms within each MoO_4 pyramidal fragment is presented.

EXPERIMENTAL

Preparative Procedures

All operations were carried out under argon in small sized Schlenk glassware equipped with high vacuum stopcocks. Spectroscopic grade D_2O (BDH), reagent grade HCl conc. (Kemika), 3,5-diaminobenzoic acid (Fluka) were used, $(NH_4)_5Mo_2Cl_9 \cdot H_2O$ was synthesized from $Mo_2(O_2CCH_3)_4$ following the published procedure.[5] $Mo_2(O_2CCH_3)_4$ was synthesized with 90% yield conversion from MoO_3 by a modified,[6] already described method.[7] Penfield tube method[8] was used in the preliminary investigation of water content in the temperature range 25–130 °C and the vapor condensate was argentometrically tested for the presence of HCl in (**1**). DTG analysis of (**1**) and (**2**) was performed on the »Mettler 3000 » system at a rate of 5 K/min. Infrared spectra were recorded on a Perkin-Elmer FT-IR 1720-X spectrometer at 2 cm^{-1} resolution in the range 4000–220 cm^1, with the samples dispersed in mineral oil mulls between CsI plates. Electronic spectra of solvated $Mo_2(O_2CC_6H_3(NH_3^+)_2)_4$ ionic species in protic and aprotic media were recorded on the Perkin Elmer UV/VIS/NIR Spectrometer Lambda 19 in the range 250–1000 nm. Filtered bright red microcrystalline samples of (**1**) were rapidly ground and their purity was tested on the powder camera Guinier-de Wolff »Nonius model 1« at Cu-Kα wavelength. High vacuum drying of the pure

sample enhanced dehydration, and diffuse lines with decreased intensity were observed. Bulk crystalline samples of (**1**) and (**2**), moderately moistened with mother liquid, were frozen and preserved for long periods at –22 °C under argon.

Synthesis of $Mo_2(O_2CC_6H_3(NH_3)_2)_4Cl_8 \cdot 16H_2O$ (**1**)

Powdered 3,5-diaminobenzoic acid (913 mg, 6 mmol) was mixed with a solution prepared from H_2O (7.9 ml, 439 mmol) and 2.1 ml HCl conc. (HCl 25 mmol, H_2O 88 mmol). The flask was evacuated and the solution was frozen. Powdered $(NH_4)_5$ $Mo_2Cl_9 \cdot H_2O$ (619 mg, 1 mmol) was added to the frozen solution, the flask was evacuated and gently warmed to 25 °C, the suspension was stirred vigorously and rapidly cleared. The intensive red-orange coloured and viscous solution was filtered through cotton-wool, purged with argon, evacuated and slowly cooled to +3 °C. After two days, bright red pinacoid prisms were filtered, dried and stored under argon at –22 °C (770 mg, 0.56 mmol, 59% average yield, based on Mo_2^{4+}).

Anal. calcd. (found) for $C_{28}H_{68}Cl_8Mo_2N_8O_{24}$: Mo, 13.94 (14.10); Cl, 20.61 (21.30); C, 24.43 (25.93); H, 4.98 (4.69); N, 8.14 (8.63)%.

Deuterated Samples of (**1**)

Bright red microcrystalline samples of (**1**) were synthesized from solutions with D_2O / HDO ratio approx. 2:1, following the previous procedure in the H_2O matrix.

Crystal Growth of $3,5-(H_2N)_2C_6H_3CO_2H \cdot 2HCl \cdot 1/2H_2O$ (**2**) Triclinic Needles

Powdered 3,5-diaminobenzoic acid (913 mg, 6 mmol) was mixed with a solution prepared from H_2O (5.25 ml, 292 mmol) and 1.0 ml HCl conc. (HCl 12 mmol, H_2O 42 mmol). The flask was evacuated, slowly cooled and stored at 3 °C for three weeks. Over 5 mm large triclinic needles were grown. Bright grey crystals suitable for crystallographic analysis were sealed in capillary glasses together with their mother liquor.

X-ray Crystallography

Several monocrystals of $Mo_2(O_2CC_6H_3(NH_3)_2)_4Cl_8 \cdot 16H_2O$ (**1**) and $3,5-(H_2N)_2C_6$ $H_3CO_2H \cdot 2HCl \cdot 1/2H_2O$ (**2**) were examined on an »Enraf Nonius« CAD-4 diffractometer at 20 °C, using Mo-Kα_1 radiation monochromated by a graphite crystal. On filter paper dried crystals, sealed in a glass capillary, were still suitable for determining the cell constants but not for collecting the full X-ray diffraction data set and they cracked upon dehydration. A pinacoid crystal of (**1**) with dimensions $0.26 \times 0.1 \times 0.74$ mm^3 and a triclinic plate of (**2**) with dimensions $0.30 \times 0.40 \times 0.09$ mm^3 were then extracted from their cold solution and, still wet, were rapidly sealed in a glass capillary with some viscous mother liquor in order to prevent decomposition. The data of (**1**) and (**2**) were processed with the NRCVAX system of crystallographic computer programmes and corrected for Lp effects.[9] Details on crystal data and refinement are listed in Table I. A numerical absorption correction by the Gauss integration method was performed for (**1**). The structural models of compounds (**1**) and (**2**) were determined with SOLVER of NRCVAX. The coordinates of molybdenum-oxygen cage with axially located chloride anions of (**1**) and carboxylic units of (**2**) were found

TABLE I

Crystallographic data for $Mo_2(O_2CC_6H_3(NH_3)_2)_4Cl_8 \cdot 16H_2O$ (**1**) and
$3,5\text{-}(H_2N)_2C_6H_3CO_2H \cdot 2HCl \cdot 1/2H_2O$ (**2**)

Empirical formula	$C_{28}H_{68}Cl_8Mo_2N_8O_{24}$	$C_7H_{10}Cl_2N_2O_2 \cdot 1/2H_2O$
Molar mass / g mol^{-1}	1376.38	234.08
Crystal system	monoclinic	triclinic
Space group	$P2_1/c$	$P\overline{1}$
a / Å	11.0825(13)	8.695(2)
b / Å	23.983(3)	9.768(2)
c / Å	10.935(6)	13.779(3)
α / °		67.43(2)
β / °	103.04(3)	68.69(2)
γ / °		72.66(2)
Volume / Å^3	2831.5(16)	989.5(4)
Z	2	4
T / K	293(2)	293(2)
λ (Mo-Kα)	0.7107	0.7107
D_x / g cm^{-3}	1.614	1.571
D_m / g cm^{-3} (flotation)	1.60	–
Reference reflections	2 5 –1; –4 5 –1; –2 4 –1	–2 –5 –6; 2 –4 –2; –4 –2 0
Measured reflections	6168 ($\pm h$, $+k$, $+l$)	5763 ($\pm h$, $+k$, $\pm l$)
Unique data	4064	3517
Observed reflections	3467 ($F_o > 4\sigma(F_o)$)	2913 ($F_o > 4\sigma(F_o)$)
μ / cm^{-1}	8.86	6.33
Transmission factor range	0.793–0.916	–
$R(F)$	0.067	0.052
$wR^2(F^2)$	0.167	0.111
Min., max. peaks in final ΔF map (e$^-$ / Å^3)	–0.98, 0.85	–0.35, 0.37

by direct methods, the difference maps gave the positions of all non-hydrogen atoms. The refinements were continued with the SHELXL–93 system of crystallographic computer programmes.[10] The water oxygen peaks were properly located in the empty solvent regions in accordance with the principle of Babinet.[11] The coordinates of all

non-hydrogen atoms were refined anisotropically, riding and rotating hydrogen atoms were located on carboxylate ligands by constraints. Contact distances between oxygen atoms of water molecules and the surrounding lattice atoms with related Donohue angles[12] were found by the C.S.U. program.[13] Trial structures and torsion angles were searched by the PLUTON program.[14] Final difference Fourier maps of electron density were calculated and depicted using the COFOUR program of NRCVAX at 0.1 Å resolution.

RESULTS AND DISCUSSION

The Reaction Medium of $Mo_2(O_2CC_6H_3(NH_3)_2)_4Cl_8 \cdot 16H_2O$ (**1**)

Synthesis of the dimolybdenum(II,II) tetracarboxylato compound was iteratively developed with multiple considerations on kinetics, thermodynamics and structural singularities in an effort to find suitable reactants and their optimal ratio. It was found experimentally that 3,5-diaminobenzoic acid is sparingly soluble in cold water but is freely solvated and protonated in ≈ 2.5 mol dm^{-3} HCl solutions to give a double protonated zwitterionic ligand with high affinity to bind on Mo_2^{4+} dimers, while 3,5-diaminobenzoic acid sulfate is poorly soluble in cold water.

The $(NH_4)_5Mo_2Cl_9H_2O$,[5] dissolved in concentrated hydrochloric solution, is a suitable source of free $Mo_2Cl_8^4$ ions, but the competitive oxidative addition of proton to Mo–Mo quadruple bond becomes very fast in solutions with [HCl] > 6 mol dm^{-3}.[15]

$$Mo_2Cl_8^{4-} + H^+ \longrightarrow Mo_2Cl_8H^{3-}$$
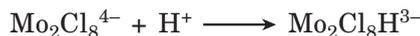
On the other side, the extent of hydrolysis rises with dilution.[16]

$$Mo_2Cl_8^{4-} + x(H_2O) \underset{\longleftarrow}{\longrightarrow} Mo_2Cl_{8-x}(H_2O)_x^{4-x} + xCl^-$$
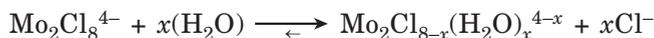
In the attempt to avoid hydrolysis and a hydrido bridged complex formation, the reaction medium was optimized in 2.4 mol dm^{-3} < [HCl] < 6 mol dm^{-3} with extending the proton addition and hydrolysis reaction intervals (up to 2.3 $t_{1/2,}$ during which the total extent of both reactions reaches 80%).[17] The pathway course of the above mentioned reactions extensively exceeded the crystal growth period of the undamaged title compound. Analogous considerations were adopted in the synthesis of $Mo_2(O_2CC_6H_3(NH_3)_2)_4Br_8 \cdot 16H_2O$ with free $Mo_2Br_8^{4-}$ substrate in 2.4 mol dm^{-3} < [HBr] < 6 mol dm^{-3} at 25 °C.

An early indication that zwitterionic 3,5-diaminobenzoate ligands can exhibit an unusually high affinity to bind on Mo_2^{4+} dimers was supported by the existence of the $\delta \longrightarrow \delta^*$ absorption peak, shifted from 520 nm (λ_{max} of

$Mo_2Cl_8^{4-}$) to 446 nm, even with ratio $[Cl^-]/[Mo_2^{4+}] \approx 15,000$ at very low concentrations of dimolybdenum tetracarboxylate (0.13 mmol dm^{-3} in 2.0 mol dm^{-3} HCl).

$$Mo_2Cl_8^{4-} + 4HO_2CC_6H_3(NH_3^+)_2 \longrightarrow$$

$$Mo_2(O_2CC_6H_3(NH_3^+)_2)_4 + 8Cl^- + 4H^+$$
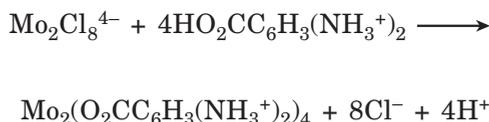
The observed absorption peak $\delta \to \delta^*$ was assigned to the zwitterionic tetrakis(3,5-diaminobenzoate)dimolybdenum(II,II) complex with double-positively charged ligands $Mo_2(O_2CC_6H_3(NH_3^+)_2)_4$ without mixed forms $Mo_2Cl_{8-2n}L_n^{(4-n)-}$, $L = {}^-O_2CC_6H_3(NH_3^+)_2$ in strongly acid aqueous solutions.

The viscous matrix solution became unstable during attempts to concentrate it on high vacuum line. When the precipitated orange powder was dehydrated on ultrahigh vacuum line at 25 °C and tested on a powder camera for crystallinity, more diffuse lines were observed, which supported the evidence of a highly charged and highly hydrated polyelectrolyte in a viscous protic matrix. A later confirmation appeared when the obtained orange powder was comparatively dissolved in DMSO at 20 °C at a concentration of 0.16 mmol dm^{-3}. The same absorption peak appeared at λ_{max} = 447 nm, so the δ bond survived intact.

The Crystal Growth of Mo$_2$(O$_2$CC$_6$H$_3$(NH$_2$)$_2$)$_4$Cl$_8 \cdot$ 16H$_2$O (1)

Therefore, the spatial arrangement of water molecules in the matrix solution was modified to obtain a highly structured and electrostricted liquid[18] with the aim to strongly compress the primary solvating solvent by the pressure effect of the electric field of the ions.[19] Isotopic effects on solvation thermodynamics by individual ionic contributions to Gibbs free energies $\Delta_{tr}G^*(S) = \Delta_sG^*(D_2O) - \Delta_sG^*(H_2O)$ for the transfer of some ionic species from light to heavy water at 25 °C were considered,[20] the remarkable differences were evaluated on $\Delta_{tr}G^*(S)$ / J mol^{-1}: 610(Cs^+, H_2O / D_2O), 295(F^-, H_2O / D_2O), 450(Cl^-, H_2O / D_2O), 780(Br^-, H_2O / D_2O) and 1050(I^-, H_2O/D_2O). The relaxation time of ultrasonic absorption amplitudes of alkali metal sulphate solutions at 5.5 °C decreases with an increase in the ionic radius[21] because of faster outer-sphere processes. The limiting conductance Λ_0 combined with Stokes equation indicates an analogous order in the decreasing degree of solvation: $r_s(Li^+) > r_s(Na^+) > r_s(K^+) > r_s(Cs^+) > r_s(NH_4^+)$

$$r_s = F^2 / 6\pi\eta N\Lambda_0^{+,-}$$

where: r_s = Stokes law radii of ions; F = Faraday constant; N = Avogadro number; Λ_0^+, Λ_0^- = limiting equivalent conductance of the ion constituents in aqueous solution; the alkali metal cations are also more solvated than ammonium ions.[22]

X-ray scattering investigations on ≈ 3.55 mol dm^{-3} (NH$_4$)$_2$SO$_4$ aqueous solutions indicate that nearly eight water molecules are arranged around the central sulphur atom[23] at about 3.8 Å. Further considerations on the first order difference neutron scattering functions and X-ray diffraction of alkali halide solutions reduced the set of usable ions.[24] Suitable counterions Cl$^-$, Br$^-$, BF$_4^-$, I$^-$, CN$^-$, N$_3^-$, Cs$^+$, and NH$_4^+$ were identified, which are known to be water »structure breaking« ions; F$^-$ and SO$_4^{2-}$ were discarded because they are recognized as water »structure making« ions.[25] Water molecules were considered to be a true reagent in the form of close packed solvent molecules or hydrated cations around the anions; therefore the coordination number 8.2 of chloride ions[26] was taken in account. A clear and homogeneous matrix solution was dimensioned preserving the stoichiometric ratio [H$_2$O] / [solvated particle] ≤ 7.8 below the previously known hydration number ≈ 8.2 of solvated chloride anions. The negative change in the self-diffusion activation energy $\Delta E_i^{\neq}$ for water exchange between the first hydration shell of Br$^-$, Cl$^-$, Cs$^+$ and NH$_4^+$ ions and the bulk solution was considered.[27] Chloride, bromide and ammonium ions are an example of negative hydration. These ions do not interact strongly with the neighbouring solvent molecules but rather increase their translational mobility. The proposed water »structure breaking« cation Cs$^+$ was properly substituted with NH$_4^+$, which has the same average distance between ion centre and the nearest water molecules in the first hydration shell.[28] Moreover, NH$_4^+$ can fit into the cavity of the structured water.[29] The starting compound (NH$_4$)$_5$Mo$_2$Cl$_9 \cdot$ H$_2$O joins all the above considerations.

An explanation of the crystal growth is now proposed according some known experimental evidence. The negative ion-pairing potential can hold together the hydrated ions, the electrostatic field of solvated ions generates a pressure on the shared water molecules within solvent-separated ion-pairs. The electrostricted water molecules are squeezed out with an expected positive change of dissolution entropy because they effectively increase the number of particles in the system.[30] At lower temperatures, all hydrogen bonds are strengthened at increased viscosity of the bulk solution. The potential energy of interacting opposite charges on ion pairs is equilibrated by the kinetic energy of random thermal motions of diffusing ions. At lower temperatures, the electrostriction becomes the prevailing phenomenon, a formed ion pair can grow up to a larger seed while free protons, which are strong »water structure making« cations, capture the squeezed water molecules from the ionic first hydration shells. The hydration number of solvated protons

raises while the original stoichiometric ratio [H$_2$O] / [hydrated ions] is forced and reduced from ≈ 7.8 to 1.0 within the growing pinacoid crystals of Mo$_2$(O$_2$CC$_6$H$_3$(NH$_3$)$_2$)$_4$Cl$_8 \cdot$ 16H$_2$O (**1**). Increasing temperature or inorganic ions in solution are considered to break up the liquid structure to some extent, since water becomes more closely packed with the increase in the percentage of hydrogen bonds broken. However, the hydrated proton H$_3$O can form hydrogen bonds with only three water molecules whose dipoles are oriented in the field of the ion. The low number of coordinated molecules and a rather open structure of hydrated proton species H$_9$O$_4^+$ could explain their little contribution of only 1.5 ml/mole to electrostriction effects[31] in comparison to 21.8 ml/mole electrostriction around OH$^-$. In the present synthesis and crystal growth, the hydrated proton is rather an acceptor of squeezed water molecules.

The Water Content within Mo$_2$(O$_2$CC$_6$H$_3$(NH$_3$)$_2$)$_4$Cl$_8 \cdot$ 16H$_2$O (1)

DTG analysis on pinacoid monocrystals revealed a continuous dehydration from room temperature with a rate maximum of water loss near 60 °C. A simple explanation became evident. At low temperatures, water molecules tend to escape from weakly binding sites, the stronger binding sites hinder the dehydration reactions also at higher temperatures. To confirm this, the deuterated title compound was synthesized in a reaction medium of a ratio [D$_2$O] / [H$_2$O] $\approx$ 2. The asymmetric HOD molecule was used as a probe,[32] which originated a simpler infrared spectrum with two equal but strong and distinct maxima of uncoupled v(O–H) and v(O–D) stretching frequencies at 3407 cm^{-1} and 2528 cm^{-1}. The estimated maximum at 3407 cm^{-1} of a D$_2$O / H$_2$O bulk solution was shifted to 3346 cm^{-1} in the obtained deuterated product. The respective difference $\Delta v = 61$ cm^{-1} was correlated to the average hydrogen bond strength of the interstitial water molecules. The electric field of cations and anions displaces the positive and negative charges in the OH and OD bonds of the HOD microphase formed in the crystal lattice. The ion-induced dipole interaction free energy $w(r)$, given by the temperature-dependent function

$$w(r) = - \{(ze)^2 \ / \ 2(4\pi\varepsilon_o\varepsilon)^2 r^4\} \ (\alpha_o + \mu_o{}^2 \ / \ 3kT)$$

with included Debye-Langevin terms of electronic and orientational polarizability, relocalizes the lone-pair density on HOD oxygen atoms and lowers the v(O–H) stretching frequency of HOD oscillators. The involved frequency shift Δv is proportional to the square of the polarizing field of a neighbour ionic charge (*ze*). These considerations support the existence of some strongly binding sites in accordance with DTG data on hindered dehydration and

high temperature water retention. The subsequent refinements of all water site occupation factors confirmed the existence of strongly and weakly occupied water sites.

The Structure of $Mo_2(O_2CC_6H_3(NH_3)_2)_4Cl_8 \cdot 16H_2O$ (**1**)

The representation of the $Mo_2(O_2CC_6H_3(NH_3^+)_2)_4Cl_2$ unit giving the atom numbering scheme is shown in Figure 1. Selected bond distances and angles are given in Table II.

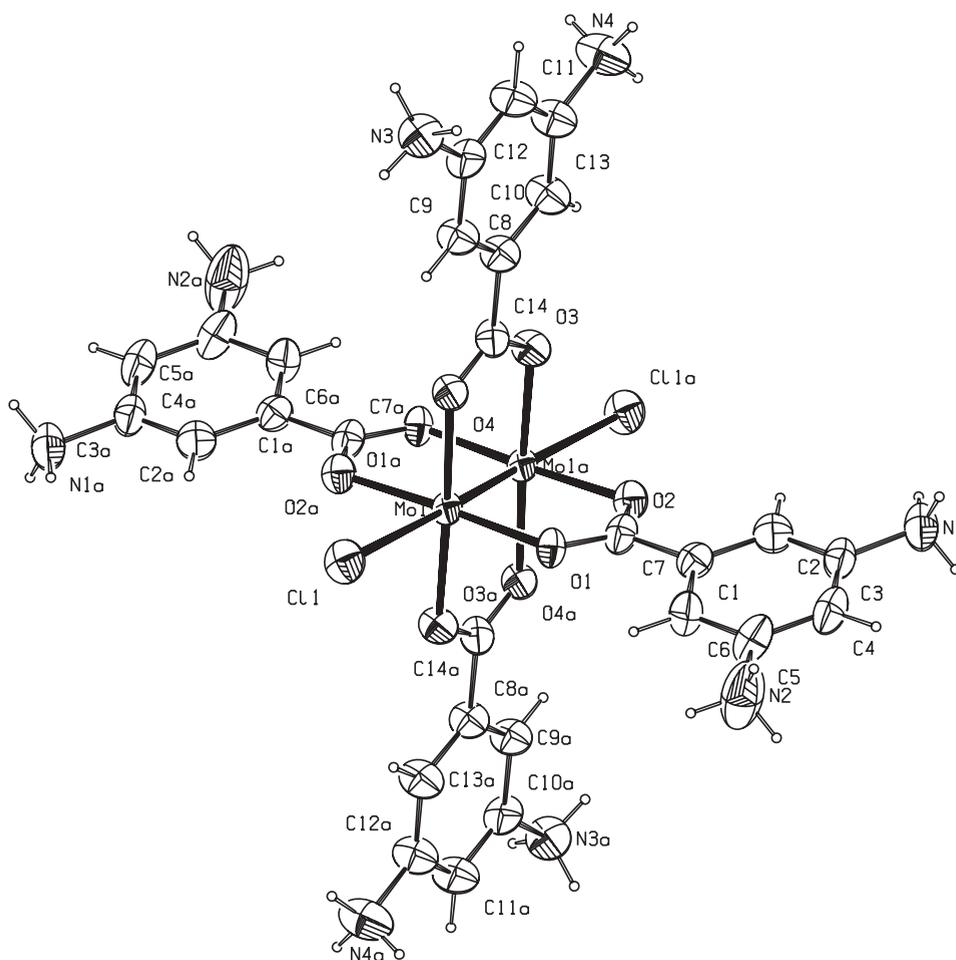Figure 1. ORTEP view of a dimolybdenum(II,II) $Mo_2(O_2CC_6H_3(NH_3^+)_2)_4Cl_2$ unit with equatorial 3,5-diaminobenzoate zwitterions and axially coordinated chloride anions.

TABLE II

Bond distances and angles in $Mo_2(O_2CC_6H_3(NH_3)_2)_4Cl_8 \cdot 16H_2O$ (**1**)[a]

Bond lengths / Å			
Mo1–Mo1'	2.1071(10)	C7–C1	1.478(11)
Mo1–O1	2.116(5)	O3–C14	1.279(9)
Mo1–O2	2.109(5)	O4–C14	1.253(9)
Mo1–O3	2.093(5)	C14–C8	1.506(11)
Mo1–O4	2.118(5)	N1–C3	1.452(11)
Mo1–Cl1	2.854(2)	N2–C5	1.454(11)
O1–C7	1.268(5)	N3–C10	1.484(10)
O2–C7	1.268(5)	N4–C12	1.474(11)
Bond angles / deg			
Mo1'–Mo1–Cl1	178.08(16)	Cl1–Mo1–O2	87.66(14)
Mo1'–Mo1–O1	91.24(13)	Cl1–Mo1–O3	90.02(15)
Mo1'–Mo1–O2	92.12(14)	Cl1–Mo1–O4	86.28(15)
Mo1'–Mo1–O3	91.88(14)	O1–C7–O2	123.2(7)
Mo1'–Mo1–O4	91.82(15)	O3–C14–O4	124.7(7)
Mo1–O1–C7	117.0(4)	O1–C7–C1	118.1(5)
Mo1–O2–C7	116.5(4)	O2–C7–C1	118.8(5)
Mo1–O3–C14	116.1(5)	O3–C14–C8	115.1(7)
Mo1–O4–C14	115.5(5)	O4–C14–C8	120.2(7)
O1–Mo1–O2	176.6(2)	C2–C1–C6	119.2(8)
O3–Mo1–O4	176.3(2)	C2–C1–C7	121.5(7)
O1–Mo1–O3	89.9(2)	C6–C1–C7	119.3(7)
O1–Mo1–O4	90.5(2)	C13–C8–C9	120.9(7)
O2–Mo1–O3	89.2(2)	C13–C8–C14	120.0(7)
O2–Mo1–O4	90.02(2)	C9–C8–C14	119.1(7)
Cl1–Mo1–O1	89.02(14)		

[a] Estimated standard deviations in the least significant digits are given in parentheses. Coordinates of primed atoms are related to those of the corresponding unprimed atoms by the transformation, $-x+1$, $-y+2$, $-z$.

Inside the carboxylate oxygen cage, the equiprobability ellipsoids of Mo(1) atoms are markedly anisotropic, the value of the anisotropic thermal displacement factor U_{22} (0.035 Å^2) being twice greater in one direction than in the other given by U_{33} (0.017 Å^2). The related environment asymmetry around the single Mo(1) atom promotes distinguished vibrations at the corners of the polyhedral cage of carboxylate oxygen atoms, as properly sug-
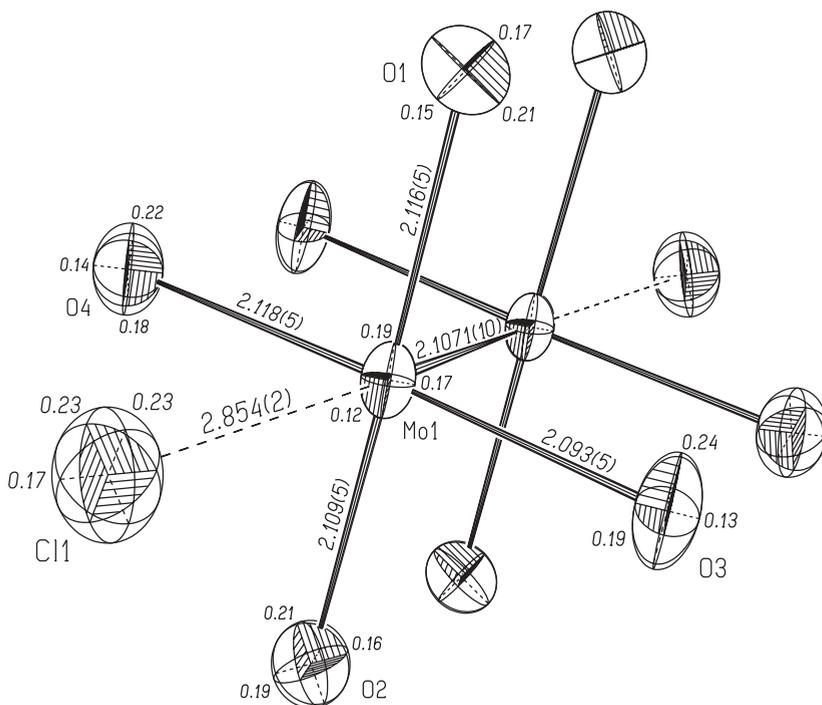
Figure 2. ORTEP view of equatorial oxygen atoms by residual thermal ellipsoids at the 50% equiprobability level, with principal values of RMS displacement in Å. Two chloride anions neutralize the slight residual charges on coaxially trapped dimolybdenum(II,II) dimer.

gested by the thermal ellipsoids in Figure 2. Three infrared absorption bands, at $v_1 = 342$ cm^{-1}(m), $v_2 = 484$ cm^{-1}(m), and $v_3 = 165$ cm^{-1}(m), were observed and assigned as suggested previously[33] to molybdenum–oxygen vibrations. Then, two non-equivalent carboxylate groups in the asymmetric unit were observed: the first one with O(1) and O(2) atoms having less marked mean square displacements and nearer carbon–oxygen distances (1.268(5), 1.268(5) Å), the second one with O(3) and O(4) atoms having visibly greater mean square displacements and nearly 3σ different carbon–oxygen distances (1.279(9), 1.253(9) Å). The longest axis vector **V1** of the thermal ellipsoid of O(3) atom with the most prominent mean square displacement $\langle u_1^2 \rangle$ is perpendicular both to the shortest molybdenum–oxygen distance 2.093(5) Å and to the longest carbon–oxygen distance 1.289(5) Å. The carbon atom C(14) shows a strong preference to vibrating along $\approx 56.0°$ out of its sp^2 plane with librational motions about the appropriate covalent bonds, so the whole carboxylate group O(3)C(14)O(4) with pronounced anisotropic motions does not make rigid body vibrations. The preferred mode of C(7) is

only $\approx 9.6°$ out of its sp^2 plane while the divergence angle between the most prominent displacements of O(1) and O(2) atoms is reduced to $\approx 5.4°$, so the scarcely pronounced anisotropic vibrations of the rather compact carboxylate group O(1)C(7)O(2) promote rigid body modes about the longitudinal main axis of the equatorially coordinated Mo(1)–Mo(1^{iii}) dimer. These observations distinguish the O(1)C(7)O(2) carboxylate group as being more ionized in comparison to the O(3)C(14)O(4) carboxylate group which neutralizes more effectively the positive charge on Mo(1) atom through the shortest Mo(1)–O(3) bond by electron donation from the more ligating O(3) atom. The exemplified aspects on differently bonded ligands suggested how to avoid a straightforward approximation of the whole oxygen cage to a librating rigid-body about its centre of inertia.

The pronounced environment asymmetry around the single molybdenum atom of the title compound was compared with an analogous asymmetric distribution of oxygen atoms inside the structure of dimolybdenum(II,II) tetra-acetate[34] $Mo_2(O_2CCH_3)_4$ and tetrapivalate[35] $Mo_2(O_2CC(CH_3)_3)_4$ in the α-form. Comparatively shorter Mo–O$_i$ averaged distances are observed within $Mo_2(O_2CC_6H_3(NH_3^+)_2)_4$ in comparison with $Mo_2(O_2CCH_3)_4$ or $Mo_2(O_2CC(CH_3)_3)_4$, as presented in Table III.

TABLE III

Comparison of averaged values of Mo(1)–O$_i$ distances

Mo(1)–O$_i$ mean distances / Å	Equatorially bonded ligands
2.109(5)	$^-O_2CC_6H_3(NH_3^+)_2$[a]
2.111(5)	$^-O_2CC(CH_3)_3$[b]
2.119(4)	$^-O_2CCH_3$[c]

[a] This work. [b,c] Calculated means from data within Ref. 34 and Ref. 35a,b.

The pivalic methyl groups exert a cumulative inductive $+I$ effect, which is higher than the analogous $+I$ effects given by smaller hydrogen atoms in acetate ligands. The observed differences between equatorial distances Mo–O$_i$ can be explained by presupposed $+I$ effects along the chain of σ bonds between carbon atoms inside the coordinated ligands. The strengthened bond between the acidic hydrogen atom and the oxygen atom in acetic acid (pK_a = 4.75) constitutes an analogous example of inductive $+I$ effects exerted by electron releasing methyl groups, so weaker inductive $+I$ effects in free formic acid lead to a stronger electrolyte (pK_a = 3.75). The free pivalic acid is a weaker electrolyte than acetic acid but the free symmetric diaminobenzoic acid is comparatively the weakest (pK_a = 5.32). The inductively enriched

charge on oxygen atoms potentiates the π donicity of bidentate carboxylic groups, strengthens the Mo–O_i equatorial bonds and shortens their interatomic distances. The zwitterionic 3,5-diaminobenzoate ligands are strongly tied through their equatorially bonded oxygen atoms in comparison with acetate or pivalate groups and more effectively shield the positive nuclear charge of central molybdenum atoms. The less ionized carboxylate group O(3)C(14)O(4), with enlarged residual electron density in the centre of the O(4)C(14) bond, lies almost coplanar with the nearest carbon atoms C(9)C(8)C(13). From values of interatomic distances listed in Table II, it emerges that the central dimer Mo_2^{4+} most intensively interacts with the ligand group O(3)C(14)O(4). Shorter equatorial Mo–O_i distances are correlated with the coplanar orientation of benzene ring and its less ionized carboxylate group because of enhanced d-π interactions between the molybdenum and oxygen electrons. The difference between refined distances Mo(1)–O(3) and Mo(1)–O(4) reaches 5σ. A torsion angle of 13.9(9)° appears between the plane of the more ionized carboxylate group O(1)C(7)O(2) and the nearer plane of endocyclic atoms C(2)C(1)C(6) which include the *ipso* atom C(1). The plane of less ionized group O(3)C(14)C(4) experiences an analogous but narrower torsion angle 1.5(14)° with the plane of endocyclic atoms C(13)C(8)C(9) that define the *ipso* atom C(8). A schematic drawing and comparisons of the above defined torsional angles are given in Figure 3, *ipso* carbon atoms C(1) and C(8) are defined in Figure 4. The different torsion angles 13.9(9)° and 1.5(14)°, which were refined inside the title compound $Mo_2(O_2CC_6H_3(NH_3)_2)_4Cl_8 \cdot 16H_2O$, were compared with an analogous
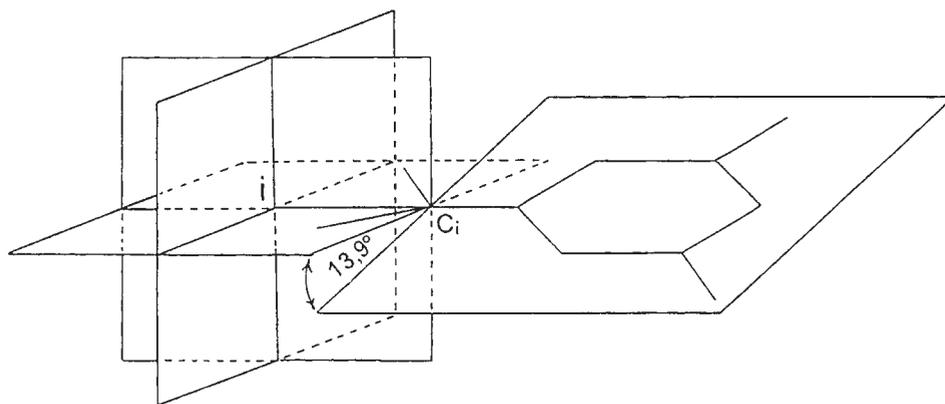

Figure 3. Schematic example of interplanar torsional angle between equatorially coordinated carboxylate group O(2)C(7)O(1) (more ionized) and protonated 3,5-diaminobenzoate ring in the asymmetric unit. Comparatively: O(3)C(14)O(4) (less ionized) with 1.5(14)°.
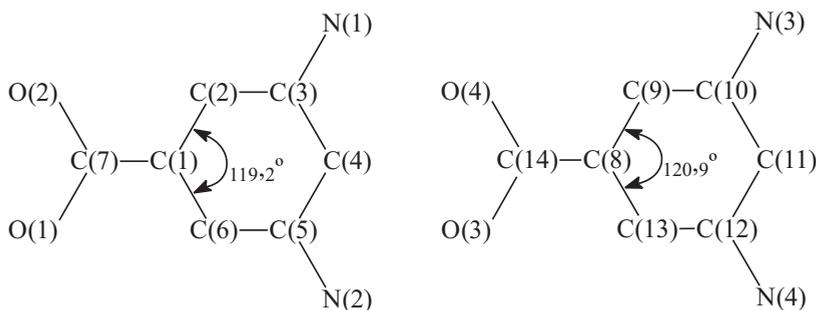
Figure 4. Lettering of C atoms and comparison of *ipso* endocyclic angles in substituted benzene rings of equatorially non-equivalent ligands.

torsion angle 8.9(5)° of the uncoordinated carboxylic group in the reference compound (**2**). The observed values 13.9(9)° > 8.9(5)° > 1.5(14)° give an indication on the relative ionization charge of the coordinated O(1)C(7)O(2) and O(3)C(14)O(4) carboxylate groups or uncoordinated carboxylic group in $HO_2CC_6H_3(NH_3^+)_2$.

Electrostatic repulsive interactions between charged oxygen atoms of O(1)C(7)O(2) carboxylate group and the nearest π electrons of the adjacent ring promote the observed torsion of the planes. The localized positive charges in the nucleus of carbon atoms and the negative charges of π electrons are not coincident in space, so the resulting electrostatic potential is not zero but rather varies with $1/r^3$ and approximates a steep potential of a quadrupole. Contributions from the lone pair regions around the charged oxygen atoms approximate a potential, that varies with $1/r$ and is still significant in long range interactions. Repulsive electrostatic fields in opposed configuration hinder the low frequency wagging motions of charged oxygen atoms and more spherical ellipsoids of O(1) and O(2) are also observed. More extensive d-π interactions between Mo(1) ↔ O(4[iv]) and Mo(1[iii]) ↔ O(3[iv]) lower the highest degree of charge on ligand atoms O(3) and O(4) in accordance with the observed interplanar torsional angle 1.5(14)° between the less ionized O(3)C(14)O(4) group and its vicinal but completely protonated 3,5-diaminobenzoate ring. In the free carboxylic group of (**2**), the electronic density is rather localized and concentrated inside the interatomic space of unionized hydroxylic and carbonylic groups and therefore the related torsion angle reaches 8.9(5)°.

Among the most reliable and indicative structural parameters of the skeletal deformations inside analogous benzoic ligands emerge modifications of the linear endocyclic angle α_x, where the *ipso* atom C_i is linked to the exocyclic[36] substituent X. The atomic thermal vibrations produce some

systematic effects, which however modify the refined interatomic distances but their influence over the interatomic angular structural parameters is less prominent.[37] Inside $Mo_2(O_2CC_6H_3(NH_3)_2)_4Cl_8 \cdot 16H_2O$ (**1**), the coordinated groups O(1)C(7)O(2) and O(3)C(14)O(4) constitute the exocyclic substituent X linked on *ipso* atoms C(1) and C(8), which define the endocyclic angles C(2)C(1)C(6) ≈ 119.2(8)° or C(13)C(8)C(9) ≈ 120.9(7)° in Figure 4.

The endocyclic angle C(13)C(8)C(9) approaches the mean values ≈ 120.7(3)° of an analogous internal angle at the *ipso* carbon atom inside the reference compound $3,5\text{-}(H_2N)_2C_6H_3CO_2H \cdot 2HCl \cdot 1/2H_2O$ (**2**) where the unionized carboxylic groups are oriented almost in the same plane with their aromatic ring. The congruent accordance of the observed and compared endocyclic angles α_x at their respective *ipso* atoms C_i confirms the existence of a lower ionization degree on the equatorially coordinated group O(3)C(14)O(4) and justifies the presupposed π interactions between oxygen ligands and the central dimer Mo_2^{4+}. The almost coplanar orientation of the carboxylate group O(3)C(14)O(4) and its vicinal atoms C(9)C(8)C(13) on the ring really potentiate the π dative influence from the ligand to the attractive centre of the molybdenum core and indirectly share the bonding distance shortening of Mo–O$_3$ and Mo–O$_4$ pairs to d_{mean} ≈ 2.106(5) Å. On the other hand, the interplanar torsion of the most ionized group O(1)C(7)O(2) lowers the neighbouring dative influence from the vicinal ring and the averaged interatomic distance of Mo–O$_1$ and Mo–O$_2$ pairs is somewhat longer d_{mean} ≈ 2.113(5) (Å). The torsional-repulsive interactions between the charged carboxylate group O(1)C(7)O(2) and vicinal π electrons of the aromatic ring involve some desymmetrization of the sp^2 hybrid at the *ipso* carbon atom C(1) and perceivable narrowing of the endocyclic angle C(2)C(1)C(6) from 120.9(7)° to 119.2(8)°. The bound oxygen atoms O(3) and O(4) around Mo_2^{4+} weaken the π bond strength inside the carbonyl C(14)O(3) group at the extent of π interactions between equatorial oxygen atoms and the central dimer Mo_2^{4+}. Further evidence of equatorial d-π interactions emerges from the difference between the shorter bond 1.199(5) Å of the free carbonyl group inside the reference compound (**2**) and the slightly longer bond 1.253(9) Å of the coordinated carbonyl group O(3)C(14) within compound (**1**). The π bond of the O(3)C(14) carbonyl group appears accordingly weakened by enhanced d-π interactions through the Mo(1)–O(4) atoms. The explored environment around positively charged nitrogen atoms reveals the existence of different contacting groups: chloride anions and clusters of water molecules structured in a crystalline microphase neutralize the positive charge on protonated amino groups. A larger number of vicinal water molecules at shorter contact distances surround the nitrogen atoms N(1) and N(2), as reported in Table IV.

TABLE IV

Donor–acceptor distances involving the NH_3^+ substituent in
$Mo_2(O_2CC_6H_3(NH_3)_2)_4Cl_8 \cdot 16H_2O$ (**1**)[a]

D–A distances / Å			
$N(1) \cdots Cl(3^{xi})$	3.099(8)	$N(3) \cdots Cl(3)$	3.150(8)
$N(1) \cdots Cl(1)$	3.215(8)	$N(3) \cdots Cl(4)$	3.09(1)
$N(1) \cdots H_2O(1)$	2.87(1)	$N(3) \cdots Cl(1^{viii})$	3.156(8)
$N(2) \cdots Cl(2^{v})$	3.145(9)	$N(4) \cdots Cl(2^{vi})$	3.259(8)
$N(2) \cdots H_2O(3)$	2.68(2)	$N(4) \cdots Cl(2^{ii})$	3.135(8)
$N(2) \cdots H_2O(4)$	3.10(2)	$N(4) \cdots H_2O(5^{vi})$	2.85(2)
$N(2) \cdots H_2O(7)$	3.10(2)	$N(4) \cdots Cl(4^{vi})$	3.39(2)

[a] Estimated standard deviations in the least significant digits are given in parentheses. Coordinates of primed atoms are related to those of the corresponding unprimed atoms by the transformations: (ii) $- x+1$, $-y+1$, $-z$; (v) $x-1$, y, z; (vi) $-x+1$, $y+0.5$, $-z+0.5$; (viii) x, $-y+1.5$, $z+0.5$.

The lone pairs of water molecules strongly interact with some acidic hydrogen atoms and promote a clean differentiation between protonated ligands within the asymmetric unit of compound (**1**), as shown in Figure 5. I.R. spectroscopic manifestations of NH antisymm. and symm. stretch. at 3593 and 3494 cm^{-1} were detected accordingly at the longest CNH_3^+ distance 1.471(5) Å between aromatic carbon atoms and full protonated amino groups in the solved structure of the reference hemihydrate (**2**). On the other hand appreciably shorter CN bond lengths of 1.452(11) Å and 1.454(12) Å in comparison to 1.474(11) Å and 1.484(10) Å are given within equatorial ligands of (**1**). A broad peak with a maximum at 3356 cm^{-1} appears in the region of shifted NH antisymm. and symm. stretching frequencies of (**1**). Protons in thermal equilibrium at ordinary temperatures have a de Broglie wavelength (if they have kinetic energy in two degrees of freedom):[38]

$$h \, / \, mv \, = \, h \, / \, (2mkT)^{1/2} \, = \, 30.8 \, / \, T^{1/2} \text{ at } 20 \text{ °C} \rightarrow \lambda \approx 1.8 \text{ Å}$$

This estimation gives a value comparable with the found interatomic distances. The proton tunneling phenomena between $-NH_3^+$ and H_2O or Cl^- in the neighbouring water-microphase release the free amino groups $-NH_2$, which leads to a small shift in the average length of C–N bonds. The impulsive $+I$ inductive effect from released $-NH_2$ groups to vicinal aromatic rings promotes enhanced and intermittent $(p\text{-}d)\pi$ donor interactions from equatorial carboxylate groups to the attractive dimolybdenum(II,II) core. A shorter equatorial $Mo-O_i$ mean distance 2.109(5) Å was observed in comparison with 2.111(5) Å or 2.119(4) Å mean distances in tetrapivalate and tetraace-
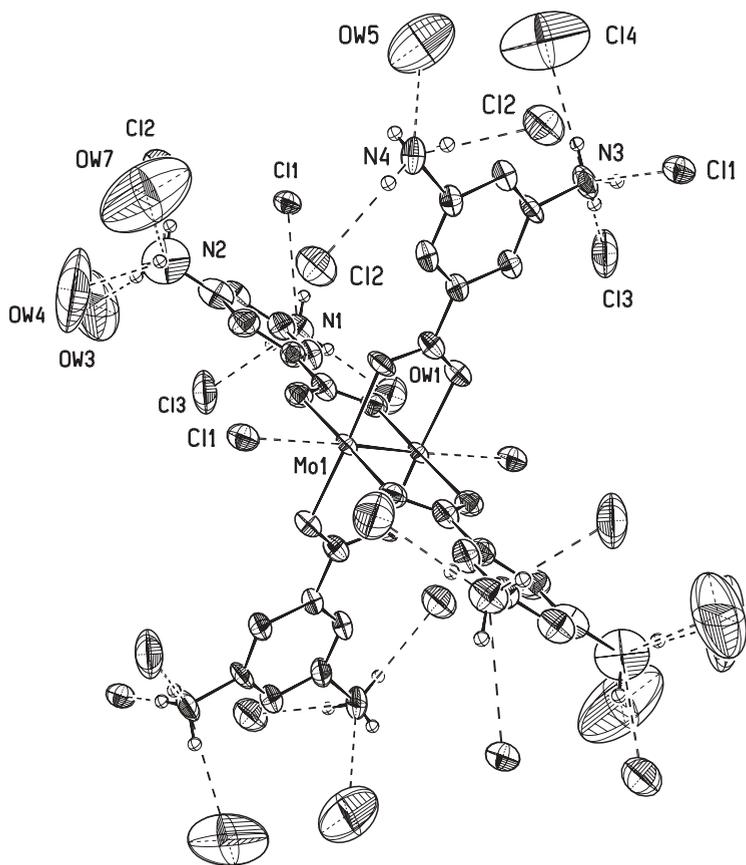
Figure 5. ORTEP view of the existence of different contacting groups in $Mo_2(O_2CC_6H_3$-$(NH_3)_2)_4Cl_8 \cdot 16H_2O$. Chloride anions and clusters of water molecules neutralize the positive charge on protonated amino groups.

tate compounds. This confirms the enhanced shielding effect of oxygen charges around Mo atoms with a slight lengthening of the dimolybdenum quadruply bond 2.1071(10) Å in comparison with the previously known 2.088(1) Å, 2.0934(8) Å, 2.096(1) Å bond lengths in tetrapivalate, tetraacetate and tetrabenzoate complexes. A net differentiation between equatorial ligands is visible in Figure 6. The d-π interactions are really important and potentiate the donor properties of $^-O_2CC_6H_3(NH_3^+)_2$ ions in charge transfer reactions with exceeding effects in comparison to analogous alkanoate ligands:[39]

$$ArCOO^- + M^{2+} \longrightarrow ArCOO^{\cdot} + M^+$$
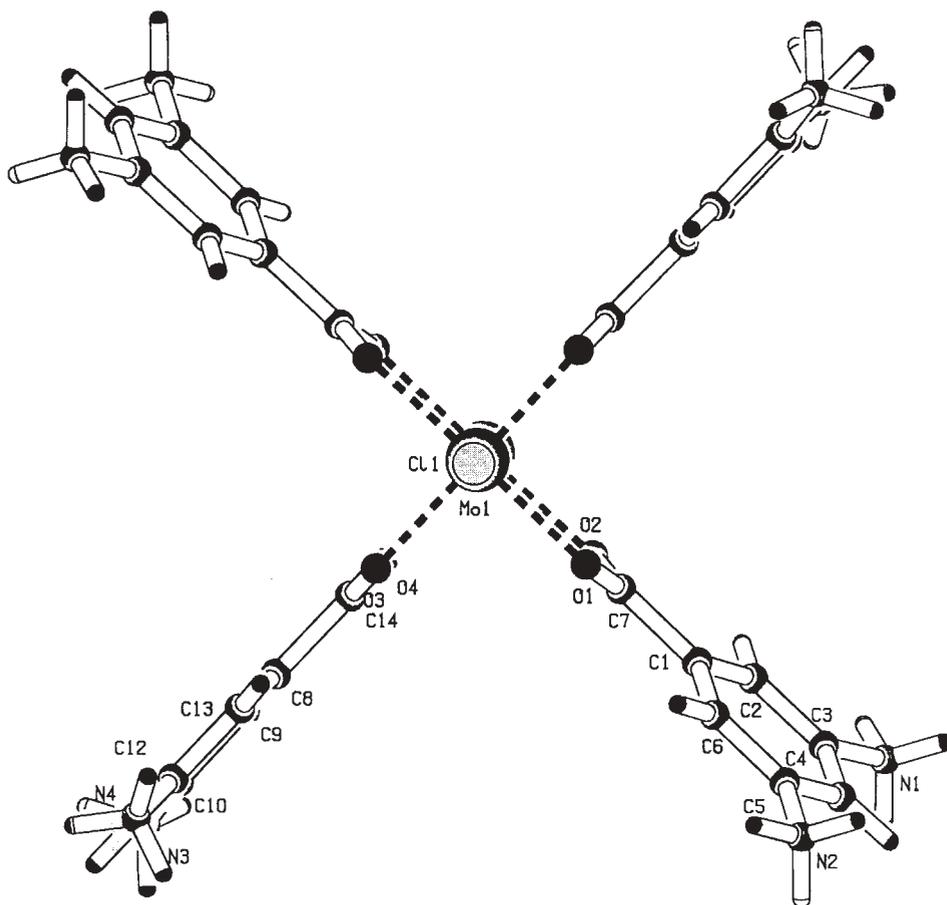
Figure 6. Distinguished interplanar torsions reveal the anomalous properties of equatorially bonded ligands in $Mo_2(O_2CC_6H_3(NH_3^+)_2)_4Cl_2$ ionic species.

In this respect, the d-π interactions reduce the formal value of the oxidation number on molybdenum atoms, so the properties of dimer Mo_2^{4+} approach the molecular entity Mo_2.

The weak δ component of the quadruple Mo(1)–Mo(1^{iii}) bond generated from a lateral overlap of metal d_{xy} orbitals favours the observed full eclipsed conformation of oxygen ligands instead of a staggered conformation »checkmated« by weaker dipole-dipole repulsive interactions between more distant Mo(1)–O_i and Mo(1^{iii})–O_i pairs of two opposed $Mo(1)O_4$ and $Mo(1^{iii})O_4$ fragments. Therefore, the related σ and π bonding components are not enhanced and the dinuclear bond length is not shortened on going from the eclipsed to staggered conformation, as the »checkmated« structure[40] of ditechnetium

compound $K_2[Tc_2Cl_6]$ suggests. Each $Mo(1)O_4$ fragment was found to be nearly square planar with a relaxed pyramidality angle $\alpha \approx 92°$, so the more diffuse and less overlapping metal d_{xz} and d_{yz} orbitals were expected to be little hybridized with metal $p_{x,y,z}$ orbitals. The molybdenum core is only partially shielded and the weak positive axial field is balanced by the cork effect of the negatively charged chloride anion $Cl(1)$.

New developments in the existence of true asymmetric dimolybdenum(II,II) core Mo_2O_8 appear to be feasible from the consideration that a large number of abundant isotopes $^{92}Mo(14.8\%)$, $^{94}Mo(9.3\%)$, $^{95}Mo(15.9\%)$ $^{96}Mo(16.7\%)$, $^{97}Mo(9.6\%)$, $^{98}Mo(24.1\%)$, $^{100}Mo(9.6\%)$ of the molybdenum element and the presence of two molybdenum atoms in the molecular dimer Mo_2 lead to a congruent differentiation between the two core fragments $Mo(1)O_4$ and $Mo(1^{iii})O_4$, their mirror images being indeed broken.

On the Structure Determination
of 3,5-$(H_2N)_2C_6H_3CO_2H \cdot 2HCl \cdot 1/2H_2O$ (2)

The reference compound 3,5-diaminobenzoic acid—bis(hydrogen chloride)—hemihydrate (2) crystallizes in the $P\overline{1}$ space group from highly solvating hydrochloric solutions. A summary of crystal data is given in Table I. Selected bond distances are given in Table V. The atom numbering scheme is shown in Figure 7. Two crystallographically independent non-zwitterionic cations $HO_2CC_6H_3(NH_3^+)_2$ with uncharged carboxyl groups are alternatively stacked along the a axis. The unusual feature of the crystal structure is the absence of carboxylic dimers, moreover the unionized carboxyl groups are twisted by about 8.9(5)° relative to their vicinal benzene ring. More stable synplanar carboxylic conformers in juxtaposition arrangement constitute the observed asymmetric unit. On the other hand, the intermolecular (hydroxyl)O–H⋯O(carbonyl) hydrogen bonding between stacked monomers is hindered. Some previously reported considerations on the infrared spectrum of gaseous monomeric formic acid[41] confirm the increased stability of synplanar structures over antiplanar conformations. It is noteworthy that the three-dimensional stacking arrangements of carboxyl dimers are the prevailing characteristics of substituted benzoic acids.[42] The observed sandwiched stacks of crystallographically independent non-zwitterions are jointed together by short contacts between paired $HO_2CC_6H_3(NH_3^+)_2$ building units. This is an example of $NH_3^+\cdots O$(carbonyl) interconnection interactions at 2.852(4) Å and 2.883(4) Å distances *via* antiparallel tail-headgroup links. The approached units $HO_2CC_6H_3(NH_3^+)_2$ are opposite each other and pivoted into antiparallel arrangements by repulsive and stretching forces between positively charged –NH_3^+ groups located on distal aromatic rings.

TABLE V

Bond distances and angles in $3,5\text{-}(H_2N)_2C_6H_3CO_2H \cdot 2HCl \cdot 1/2H_2O$ (**2**)[a]

| Bond lengths / Å			
O(1)–C(1)'	1.310(5)	N(1)–C(3)	1.468(4)
O(2)–C(1)'	1.199(5)	N(2)–C(5)	1.466(4)
C(1)'–C(1)	1.498(5)	N(3)–C(11)	1.459(4)
O(3)–C(7)'	1.315(5)	N(4)–C(9)	1.471(5)
O(4)–C(7)'	1.200(4)	O_W–H(21)	0.96(3)
C(7)'–C(7)	1.498(5)	O_W–H(22)	0.96(3)
Bond angles / deg			
O(1)–C(1)'–O(2)	124.0(4)	C(6)–C(1)–C(2)	120.7(3)
O(3)–C(7)'–O(4)	124.2(3)	C(8)–C(7)–C(12)	120.5(3)
O(1)–C(1)'–C(1)	113.5(3)	H(21)–O_W–H(22)	105.5(8)
O(2)–C(1)'–C(1)	122.4(3)	C(1)'–O(1)–H(19)	109.5(2)
O(3)–C(7)'–C(7)	113.5(3)	C(7)'–O(3)–H(20)	109.5(2)
O(4)–C(7)–C(7)	122.3(3)		
Dihedral angles / deg			
O(1)–C(1)'–C(1)–C(2)	−172.1(4)	O(3)–C(7)'–C(7)–C(8)	−7.2(6)
O(1)–C(1)'–C(1)–C(6)	9.0(6)	O(3)–C(7)'–C(7)–C(12)	171.8(4)
O(2)–C(1)'–C(1)–C(2)	7.1(6)	O(4)–C(7)'–C(7)–C(8)	172.2(4)
O(2)–C(1)'–C(1)–C(6)	−171.9(4)	O(4)–C(7)'–C(7)–C(12)	−8.9(6)
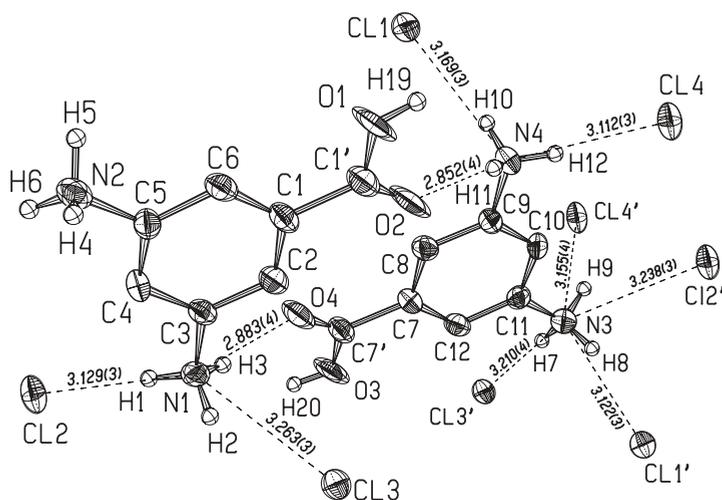
Figure 7. ORTEP view of the atom numbering scheme and donor acceptor distances involving the NH$_3$ substituent in the asymmetric unit of $3,5\text{-}(H_2N)_2C_6H_3CO_2H \cdot 2HCl \cdot 1/2H_2O$ hemihydrate.

Supplementary materials. – Crystallographic data for the structures reported in this paper have been deposited with the Cambridge Crystallographic Data Centre, 12 Union Road, Cambridge, CB2 1EZ, UK (fax: +44-1223-336033; e-mail: deposit@ ccdc.cam.ac.uk) and can be obtained on request, free of charge, by quoting the publication citation and the deposition numbers 102897 (**1**) and 102898 (**2**).

REFERENCES

1. (a) G. Snatzke, U. Wagner, and H. P. Wolff, *Tetrahedron* **37** (1981) 349–361;
   (b) J. Frelek and G. Snatzke, *Fresenius Z. Anal. Chem.* **316** (1983) 261–264.
2. A. Carvill, P. Higgins, G. M. McCann, H. Ryan, and A. Shiels, *J. Chem. Soc., Dalton Trans.* (1989) 2435–2441.
3. A. Ducruix, J. P. Guilloteau, M. Riès-Kautt, and A. Tardieu, *J. Cryst. Growth* **168** (1996) 28–39.
4. F. A. Cotton and J. G. Norman Jr., *J. Am. Chem. Soc.* **94** (1972) 5697–5702.
5. J. V. Brenčič and F. A. Cotton, *Inorg. Chem.* **9** (1970) 346–351.
6. B. Udovic and P. Šegedin, unpublished work.
7. A. Bino and D. Gibson, *J. Am. Chem. Soc.* **102** (1980) 4277–4278.
8. S. L. Penfield, *Am. J. Sci.* **48** (1894) 30–37.
9. E. J. Gabe, Y. Le Page, J. P. Charland, F. L. Lee, and P. S. White, *J. Appl. Crystallogr.* **22** (1989) 384–393.
10. G. Sheldrick, SHELXL-93. System of Crystallographic Computer Programmes, Institut für anorganische Chemie der Universität Göttingen, Germany, 1993.
11. (a) R. Langridge, D. A. Marvin, W. E. Seeds, H. R. Wilson, C. W. Hooper, M. H. F. Wilkins, and L. D. Hamilton, *J. Mol. Biol.* **2** (1960) 38–64;
    (b) H. Driessen, M. I. J. Haneef, G. W. Harris, B. Howlin, G. Khan, and D. S. Moss, *J. Appl. Crystallogr.* **22** (1989) 510–516.
12. J. Donohue, *J. Phys. Chem.* **56** (1952) 502–510.
13. I. Vicković, Crystal Structure Utility (C.S.U.) Program, *J. Appl. Crystallogr.* **21** (1988) 987–990.
14. A. L. Spek, PLUTON–93-(C), Display and Analysis of Crystal and Molecular Structures Program, University of Utrecht, the Netherlands, 1980–1993.
15. S. Miller, and A. J. Haim, *J. Am. Chem. Soc.* **105** (1983) 5624–5626.
16. C. Mertis, M. Kravaritou, A. Shehadeh, and D. Katakis, *Polyhedron* **6** (1987) 1975–1980.
17. (a) B. Udovic, Diploma work, University of Ljubljana, 1990;
    (b) P. Šegedin and B. Udovic, *Vestn. Slov. Kem. Druš.* **38** (1991) 195–204;
    (c) P. Šegedin and B. Udovic, *Vestn. Slov. Kem. Druš.* **39** (1992) 325–340.
18. (a) J. E. Desnoyers, R. E. Verrall, and B. E. Conway, *J. Chem. Phys.* **43** (1965) 243–250;
    (b) R. D. Feltham and R. G. Hayter, *J. Chem. Soc.* (1964) 4587–4591;
    (c) H. Falkenhagen and M. Dole, *Phys. Z.* **30** (1929) 611–622.
19. J. Padova, *J. Chem. Phys.* **39** (1963) 1552–1557.
20. Y. Marcus and A. Ben-Naim, *J. Chem. Soc.* **83** (1985) 4774–4759.
21. T. J. Gilligan and G. Atkinson, *J. Chem. Soc.* **84** (1980) 208–213.

22. J. E. Prue and P. J. Sherrington, *Trans. Faraday Soc.* **57** (1961) 1795–1808.
23. R. Caminiti, G. Paschina, and G. Pinna, *Chem. Phys. Lett.* **64** (1979) 391–395.
24. (a) J. E. Enderby and G. W. Nielson, *Rep. Prog. Phys.* **44** (1981) 593–653;
    (b) G. Licheri, G. Piccalunga, and P. Pinna, *J. Appl. Crystallogr.* **6** (1973) 392–395.
25. (a) Ref. 20; (b)Ref. 21; (c) V. V. Goncharov, I. I. Romanova, O. Ya. Samoilov, and V. I. Yashkichev, *Zh. Struct. Khim.* **8** (1967) 613–617.
26. Ref. 24b.
27. (a) M. Mezei and D. L. Beveridge, *J. Chem. Phys.* **74** (1981) 6902–6910;
    (b) Ref. 25c.
28. Y. Marcus, *J. Solution Chem.* **12** (1983) 271–275.
29. A. H. Narten, *J. Phys. Chem.* **74** (1970) 765–768.
30. (a) N. Z. Bjerrum, *Z. Anorg. Allg. Chem.* **109** (1920) 275–292;
    (b) F. J. Millero, and W. L. Masterton, *J. Phys. Chem.* **78** (1974) 1287–1294;
    (c) D. F. Evans, and M. A. Matesich, *J. Solution Chem.* **2** (1973) 193–216.
31. R. M. Noyes, *J. Am. Chem. Soc.* **86** (1924) 971–979.
32. (a) K. A. Hartman Jr., *J. Phys. Chem.* **70** (1966) 270–276;
    (b) B. Z. Gorbunov and Yu. I. Naberukhin, *Zh. Struct. Khim.* **16** (1975) 816–823.
33. A. P. Ketteringham, C. Oldham, and C. J. Peacock, *J. Chem. Soc., Dalton Trans.* (1976) 1640–1642.
34. F. A. Cotton, Z. M. Mester, and T. R. Webb, *Acta Crystallogr. Sect. B* **30** (1974) 2768–2770.
35. (a) F. A. Cotton, M. Extine, and L. D. Gage, *Inorg. Chem.* **17** (1978) 172–176;
    (b) D. S. Martin, and H. W. Huang, *Inorg. Chem.* **29** (1990) 3674–3680.
36. (a) A. Domenicano and A. Vaciago, *Acta Crystallogr., Sect. B* **35** (1979) 1382–1388;
    (b) A. Domenicano, A. Vaciago, and C. A. Coulson, *Acta Crystalloogr., Sect. B* **31** (1975) 1630–1641
37. A. Domenicano, P. Mazzeo, and A. Vaciago, *Tetrahedron Lett.* **13** (1976) 1029–1032.
38. E. F. Caldin, *Chem. Rev.* **69** (1969) 135–156.
39. D. P. Graddon, *J. Inorg. Nucl. Chem.* **17** (1961) 222–231.
40. S. V. Kryutchkov, M. S. Grigor'ev, A. F. Kuzina, B. F. Gulev, and V. I. Spitsyn, *Dokl. Akad. Nauk SSSR* **288** (1986) 389–393.
41. T. Miyazawa and K. S. Pitzer, *J. Chem. Phys.* **30** (1959) 1076–1086.
42. (a) R. S. Miller, D. Y. Curtin, and I. C. Paul, *J. Am. Chem. Soc.* **96** (1974) 6340–6349; (b) L. Leiserowitz, *Acta Crystallogr., Sect. B* **32** (1976) 775–802.

SAŽETAK

O kaotropski priređenom dimolibdenskom(II,II) spoju

Boris Udovic, Ivan Leban i Primož Šegedin

Neklasičnim pristupom pri sintezi i kristalizaciji, koristeći se pojavom elektro-strikcije u vodenim otopinama ionskih vrsta visokog naboja, priređeni su prozirni jedinični kristali zwitterionskog tetrakarboksilatnog molibdenskog spoja tetrakis-(μ-3,5-di-amino-benzoat)oktaklorodimolibden(II,II)—voda (1/16), $Mo_2[O_2CC_6H_3(NH_3)_2]_4Cl_8 \cdot 16H_2O$ (**1**). Spoj kristalizira u monoklinskoj prostornoj grupi $P2_1/c$ s parametrima

jedinične ćelije: a = 11,0825(13) Å, b = 23,983(3) Å, c = 10,935(6) Å, β = 103,04(3)° i Z = 2. Preskoci protona između aromatske –NH_3^+ i susjednih, povezujućih skupina H_2O ili Cl^- povećavaju stupanj (p-π) donorskih interakcija između ekvatorijalnih kisikovih atoma i središnje dimolibdenske(II,II) jezgre. Strukturnim određivanjem dokazano je postojanje karboksilatnih liganada nejednakih s obzirom na jakost vezanja na Mo_2^{4+} dimernu jedinku. Također je određena kristalna i molekulska struktura referentnog spoja 3,5-diaminobenzojeve kiseline—bis(klorovodik)—hemihidrata, 3,5-$(H_2N)_2C_6H_3CO_2H \cdot 2HCl \cdot 1/2H_2O$ (**2**) čiji su strukturni podaci uspoređeni s onima spoja (**1**). Igličasti kristali spoja (**2**) pripadaju triklinskom sustavu, prostornoj grupi $P\bar{1}$ i imaju ove parametre jedinične ćelije: a = 8,695(2) Å, b = 9,768(2) Å, c = 13,779(3) Å, α = 67,43(2)°, β = 68,69(2)°, γ = 72,66(2)° i Z = 4.